

Design of a Self-Folding Composite Variable-Diameter Wheel Structure based on 4D Printing Technology

Wencai Zhang¹ – Zhenghao Ge¹ – Duanling Li^{1,2,*}

¹ Shaanxi University of Science and Technology, College of Mechanical and Electrical Engineering, China

² Beijing University of Posts and Telecommunications, School of Automation, China

The conventional variable-diameter wheel's complex control system and structure seriously affect its mobility and dependability in unstructured terrain. Based on 4-dimensional (4D) printing technology, this work proposes a self-folding composite variable-diameter wheel consisting of a self-folding structure and an outer hub that can self-adjust the wheel diameter under thermal stimulation, avoiding the drawbacks of conventional structures. The structure integrates the control system and variable-diameter mechanical structure using 4D printing. The design and construction of the self-folding structures are introduced, and the mathematical model and design parameters for self-folding motion are obtained using kinematic analysis. Based on the above research and material properties analysis, a programmable morphing structural design and morphing influence investigation based on manufacturing parameters are carried out for the self-folding rod that controls the contraction of this structure. The digital model and prototype have been developed to verify the feasibility of the design and the correctness of the theoretical analysis and to realize the self-adjusting wheel diameter under thermal stimulation.

Keywords: self-folding, smart materials, 4D printing, variable-diameter wheel

Highlights

- A conventional variable-diameter wheel's complex structure is simplified using 4D printing technology to integrate the control system and the variable-diameter mechanical structure.
- A conventional variable-diameter wheel's complex control system is simplified using smart materials to control wheel diameter changes under external thermal stimulation.
- Conventional mechanical structure design, smart materials, and fabrication are integrated via 4D printing. The single mechanical structure design extends to a programmable morphing structure design.

0 INTRODUCTION

Robots have been increasingly used in aerospace, industrial production, geological exploration, and other fields. When carrying out the design of robots (except fixed-position robots), the traveling mechanism, as the crucial system for performing tasks, is mainly wheeled traveling device, legged traveling device, crawler traveling device, or composite traveling device [1] to [3]. Wheeled traveling devices are widely used because of their adaptability, reliable operation, and easy control. However, with the expanding scope of human research, engineering, and habitat, complex and harsh application scenarios require wheeled mechanisms with enhanced environmental adaptability [4]. Therefore, the variable-diameter wheel, which changes the diameter to cope with different terrain changes and improves the passing capability, has been created [5] to [7]. Commonly variable-diameter wheels can be divided according to their deformation modes: inflatable and mechanical [8] to [9]. Among these, the mechanical type gained the attention of many scholars because of its simple design concept, high stiffness, and good movement efficiency [10] to [12]. Mechanical variable-diameter wheels typically

necessitate integrating both the control system and the variable-diameter mechanical structure to switch between different environments to improve passing capability. However, these mechanical structures are often less reliable and more difficult to control due to their complex structures and control systems [13] to [15]. As a result, variable-diameter wheels must retain their original powerful passing capability while maintaining a simple structure with low control complexity and improved reliability. This urgent issue must be addressed.

The emergence of smart materials and 4-dimensional (4D) printing technology provides a new idea for the design of variable-diameter wheels. By changing smart materials' distribution and geometric parameters, combining 4D printing technology with conventional mechanical structure design methods creates a structure with a controlled self-driven deformation or transformation function under predetermined structural excitation conditions. The single mechanical structure design extends to a programmable morphing structure design. Applying this new idea will effectively circumvent the defects of the conventional variable-diameter wheel. This work's main contributions are listed as follows:

*Corr. Author's Address: Shaanxi University of Science & Technology, Weiyang District, Xi'an, China, liuanlini@163.com

1. Based on 4D printing technology, this work proposes a novel self-folding composite variable-diameter wheel structure. The structure comprises a self-folding structure and an outer hub.
2. Based on mechanical structure design methods and principles, kinematic analysis introduces to obtain a mathematical model of self-folding motion.
3. The structural design based on programmable morphing and research of morphing influence based on manufacturing parameters is conducted for the self-folding rod to control the contraction of this structure.
4. Constructed simulations and experiments achieve the drivable self-adjustment of the wheel size ratio under predetermined thermal stimuli.

1 DESIGN OF A SELF-FOLDING COMPOSITE VARIABLE-DIAMETER WHEEL STRUCTURE

This section consists of three parts. First, it gives the general design concept and operation mode of the self-folding composite variable-diameter wheel structure. Second, it introduces the composition of the core self-folding structure that attains the wheel diameter change function. Finally, there are discussions on the design differences between self-folding and conventional mechanical structures.

A self-folding composite variable-diameter wheel structure with thermally stimulated deformation response property is designed (see Fig. 1a). The structure consists of a self-folding structure (see Fig. 1c) and an outer hub (see Fig. 1b), prepared with a high-precision 3D printer.

Usually ($T < T_g$), the self-folding structure unfolds and works as a moving wheel. At that moment, the wheel diameter reaches its maximum value. Applying an external thermal stimulus ($T > T_g$), the self-folding structure contracts along the track and into the outer hub and uses the outer hub as a moving wheel. At this moment, the wheel diameter reaches its minimum value (see Fig. 1d).

The response of the self-folding structure to external thermal stimulus is crucial to attaining the change in wheel diameter. For this purpose, the self-folding rod changed from an unfolded state to a folded state according to the pre-programmed design and drives the angulated scissor rod to contract the entire structure during the traveling process (see Fig. 1d).

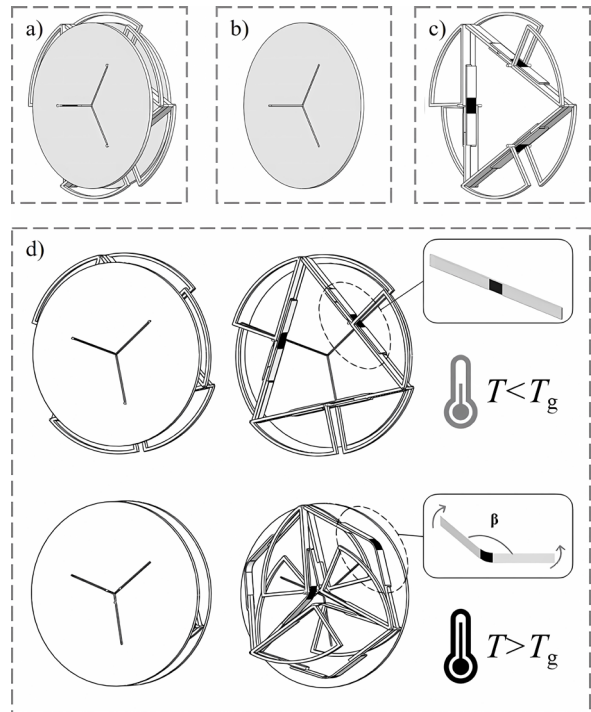


Fig. 1. Schematic; a) self-folding composite variable-diameter wheel structure, b) outer hub, c) self-folding structure, and d) structural contraction process

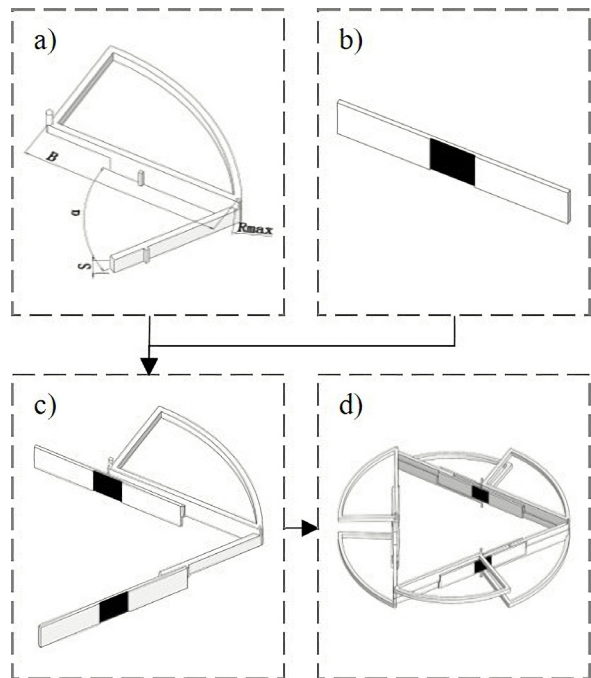


Fig. 2. Schematic of self-folding structure; a) angulated scissor rod, b) self-folding rod, c) assembly structure, and d) self-folding structure

Because of the distinct features of controlled structural transformation in response to predetermined

thermal stimuli, the critical structural design parameters and mathematical model required for deformation control need to be deduced in order to investigate the deformation control relationship between the angulated scissor rod and the self-folding rod. However, the conventional mechanical structure design method cannot be used as a single basis for this research, which aims to lay part of the foundation for the next advancement of conventional structural design to programmable morphing structural design.

2 ANALYSES OF SELF-FOLDING STRUCTURE

This section contains two subsections. First, there are analyses of the self-folding structure's design methods and structural principles. Second, kinematic analysis is carried out to obtain the equation and structural design parameters for drivable self-folding motion.

2.1 Design Method and Structural Principle

Two angulated scissor rods (dhp and bha) and two self-folding rods (tpq and uaj) are extracted from the self-folding composite variable-diameter wheel structure to establish a rectangular coordinate system (see Fig. 3a).

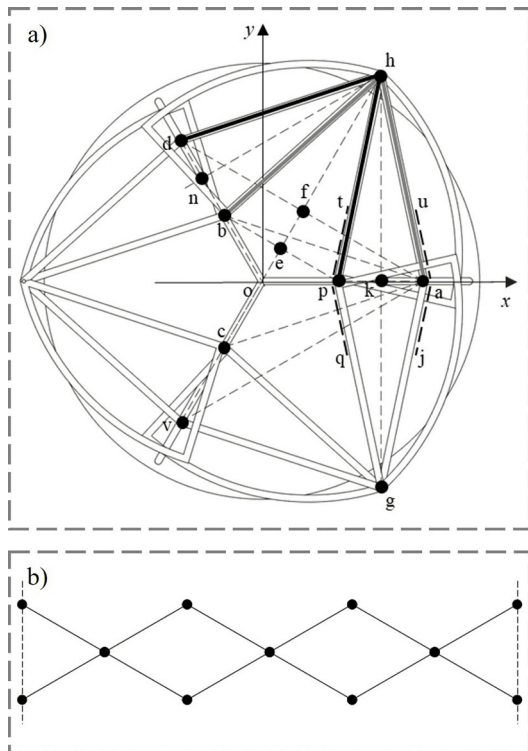


Fig. 3. Schematic, a) coordinate systems of the self-folding structure, b) structured expansion kinetic chain

The perpendicular lines are made through point h to line db and the x -axis, with the intersection points n and k . The top angle α and the length B of dhp and bha are manufacturing parameters (see Fig. 2a) whose values are constants. We can prove the following:

- $\because \angle dhp = \angle bha = \alpha$
- $\because \angle bhp$ is the common angle
- $\therefore \angle dhb = \angle dhp - \angle bhp = \angle bha - \angle bhp = \angle pha$
- $\because dh = bh = ph = ah$
- $\therefore \triangle dhb$ and $\triangle pha$ are congruent isosceles triangles
- \because The lines nh and kh are the perpendicular bisector of $\triangle dhb$ and $\triangle pha$
- $\therefore \triangle dhn = \triangle nhb = \triangle phk = \triangle kha$
- $\because \angle dhn = \angle nhb = \angle phk = \angle kha$
- $\therefore 2\angle nhb + \angle bhp = 2\angle phk + \angle bhp = \alpha$
- $\because \angle nhb + \angle bhp + \angle phk = \alpha$
- $\because \angle onh + \angle okh + \angle nhk + \angle nok = 2\pi$
- $\because \angle onh = \angle okh = \pi/2$
- $\therefore \angle nok = \angle doa = \pi - \alpha$

Let α be

$$\alpha = \pi - \frac{2\pi}{m}, \quad (m = k + 3 \wedge k \in \mathbb{Z}), \quad (1)$$

where m is the number of rod groups required to construct the self-folding structure, there are $2m$ self-folding rods and $2m$ angulated scissor rods.

The above proof concludes that the angle in a circular segment (such as $\angle doa$) corresponding to each group of angulated scissor rods is always constant. Its value is only related to the number of rod groups m . The value of m also determines the top angle α of the angulated scissor rods. Thus, using m rod groups, a ring-shaped self-folding structure can be constructed. The specific construction method is as follows (see Figs. 2 and 3): hinges connect the angulated scissor rods at the top angles h and g . The self-folding rods are bonded at the limit blocks t , v , u , and j . By analogy, a self-folding structure can be constructed consisting of m rod groups. The purpose of the limit blocks is to prevent uneven force or collision interference between the self-folding rods and the angulated scissor rods due to the inaccurate positioning of the bond.

In this work, the value of m for the designed self-folding structure is set to 3. The structure is expanded into a plane kinetic chain along the line connecting point p and point a (see Fig. 3b). Applying the loop connectivity matrix (LCM) [16], we know that:

$$\mathbf{R}_{LCM} = \begin{bmatrix} 1 & 1 & 0 & 0 \\ 0 & 1 & 1 & 0 \\ 0 & 0 & \ddots & 1 \\ 0 & 0 & 0 & m \end{bmatrix}, \quad (2)$$

Let F is the degree of freedom. According to Eq. (2):

$$F = 1 + 1 - 1 + 1 - 1 + 1 - 1 = 1.$$

From the above calculations, we conclude that the self-folding structure has single degrees of freedom.

The previous paragraph analyses the self-folding structure's design methods and structural principles. On this basis, this structure's contraction change process is explained (see Fig. 4).

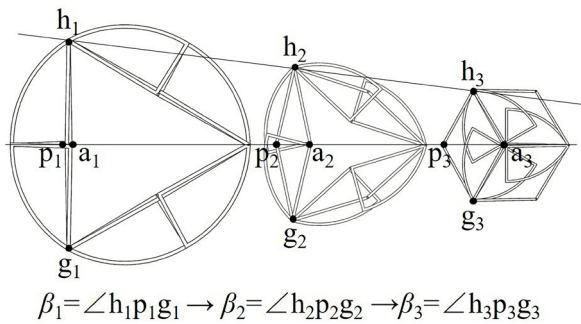


Fig. 4. Contraction process of the self-folding structure

The self-folding rod folded under external thermal stimulation, and the folding angle change process is $\beta_1 \rightarrow \beta_2 \rightarrow \beta_3$. The self-folding rod midpoint p and a move along the line pa , which drives the angulated scissor rod between the hinge point h along the path of the connecting line $h_1 h_3$ movement. The diagonal pa changes throughout the process. One large and one small circle in different states are formed by connecting a series of diagonal endpoints h in the unfolded state to a series of diagonal endpoints a in the folded state, which obtains structural contraction changes.

2.2 Kinematic Analysis

The angles hpg and hag are defined as folding angle β (see Fig. 4). The angulated scissor rod length is defined as B (see Fig. 2a).

In the triangle dha , let angle hpa is the Z , the length of the line ad is (see Fig. 3):

$$ad = 2B \cos \angle ahd = 2B \cos \left(Z - \frac{\alpha}{2} \right). \quad (3)$$

In the triangle doa ,

$$ad^2 = od^2 + oa^2 - 2od \cdot oa \cdot \cos(\pi - \alpha). \quad (4)$$

When the folding angle reaches a minimum value, the structure is contracted. Let R_{\min} be the minimum circumcircle radius. Let β_{\min} be the minimum folding angle. In the triangle doa , it can be seen that R_{\min} is equal to ao and od , bringing Eq. (3) into Eq. (4); we know that:

$$ad^2 = R_{\min}^2 + R_{\min}^2 - 2R_{\min}^2 \cos(\pi - \alpha),$$

$$ad = 2B \cos \left(Z_{\min} - \frac{\alpha}{2} \right).$$

Let Eq. (3) equal Eq. (4), and we can solve the following:

$$4B^2 \cos \left(Z_{\min} - \frac{\alpha}{2} \right) = 2R_{\min}^2 (1 + \cos \alpha). \quad (5)$$

According to Eq. (5), we can solve the following:

$$R_{\min} = B \cos \left(Z_{\min} - \frac{\alpha}{2} \right) \cos^{-1} \frac{\alpha}{2}, \quad (6)$$

$$Z_{\min} = \arccos \left(\frac{R_{\min}}{B} \cos \frac{\alpha}{2} \right) + \frac{\alpha}{2}. \quad (7)$$

Combined with Fig. 4, it can be seen that R_{\min} is equal to B . Bringing Eq. (7), we can solve the following:

$$Z_{\min} = \frac{\alpha}{2} + \frac{\alpha}{2} = \pi - \frac{2\pi}{m}, \quad (8)$$

$$\beta_{\min} = 2Z_{\min} = 2\pi - \frac{4\pi}{m}. \quad (9)$$

When the folding angle reaches a maximum value, the structure is unfolded. Let R_{\max} be the maximum circumcircle radius. Let β_{\max} be the maximum folding angle. In the triangle oha , it can be seen that R_{\max} is equal to oh ; we know that:

$$R_{\max} = B \sin^{-1} \left(Z_{\max} - \frac{\alpha}{2} \right). \quad (10)$$

Combined with Fig. 4, it can be seen that angle haf is equal to angle foa , and we can solve the following:

$$Z_{\max} - \frac{\alpha}{2} = \frac{\pi - \alpha}{2} = \frac{\pi}{2}. \quad (11)$$

$$\beta_{\max} = 2Z_{\max} = \pi. \quad (12)$$

Let χ be the structural contraction ratio, bringing Eq. (6) and Eq. (10), and we can solve the following:

$$\chi = \frac{R_{\min}}{R_{\max}} = \sin\left(\frac{\pi}{m}\right). \quad (13)$$

From the above calculations, we conclude that the m value determines the structure's construction, contraction process, and contraction ratio. As a result, the crucial structural design parameter required for deformation control is m . Taking the structure with an m value equal to 3 as an example, the contraction ratio χ of this structure is about 0.866, and its folding angle β varies from 180° to 120°.

3 PROGRAMMABLE MORPHING RESEARCH OF SELF-FOLDING RODS

In this section, we research the programmable morphing of the self-folding structure after obtaining the design method and structural principle. The self-folding rod is a component with an integrated motion actuator and driver. It is the core part that controls the contraction of the self-folding structure.

This section contains three subsections. First, it tests the thermo-mechanical properties of the materials required to manufacture the self-folding rod. Second, it researches programmable morphing based on various materials' structural design and thermo-mechanical properties. Finally, it researches the influence of folding morphing based on the adjustment of manufacturing parameters.

3.1 Characterization of Material Properties

The manufacturing and control of self-folding rods can utilize the thermo-mechanical properties of different materials. In addition, heat stimulation is used as a means of structure activation in this work. Therefore, material property tests are conducted to characterize

the material's thermo-mechanical properties and provide a relevant basis for subsequent research.

Four commercial elastomer materials are selected, thermoplastic polyurethane (TPU) (Dake, Shenzhen, China), and one shape memory polymer material, polylactic acid (PLA) (Raise Premium, Shanghai, China). The dynamic thermo-mechanical properties of these five materials are analysed using a dynamic thermo-mechanical analyser (DMA-Q800, New Castle, United States), selected tensile mode. The practical test length of the PLA and TPU printed filaments is 10 mm, and the diameter is 1.75 mm. The test loading temperature range is 25 °C to 90 °C. The accuracy of the temperature loading is ±0.2 °C. The temperature rise rate is controlled by 2 °C/min during the test. The dynamic axial stretching rate is 1 Hz. The dynamic thermo-mechanical analyser (DMA) test results (see Fig. 5) included the changes in the storage modulus G and dissipation factor angle $\tan \delta$ with temperature T . The T_i , T_g , and T_h of PLA are 61.96 °C, 68.02 °C, and 73.57 °C, respectively. The G values for PLA corresponding to the three temperatures are 2458.760 MPa, 1375.287 MPa, and 637.7503 MPa. The subscripts i , g , and h represent the beginning, transition, and end of PLA's glass transition phase. Similarly, the DMA test results for TPU show that the T_g of TPU is below room temperature, and G values of TPU decrease slowly with increasing temperature.

3.2 Structural Design Based on Programmable Morphing

The self-folding rod drives the whole structure to produce contraction by bending. Therefore, this section discusses how to program the self-folding rod to produce bending by structural design.

A self-folding rod structure based on thermal stimulus-response is designed. The structure is manufactured using a fused deposition modelling (FDM) dual-nozzle printer (Raise E2, Shanghai, China) utilizing TPU and PLA material (see Fig.

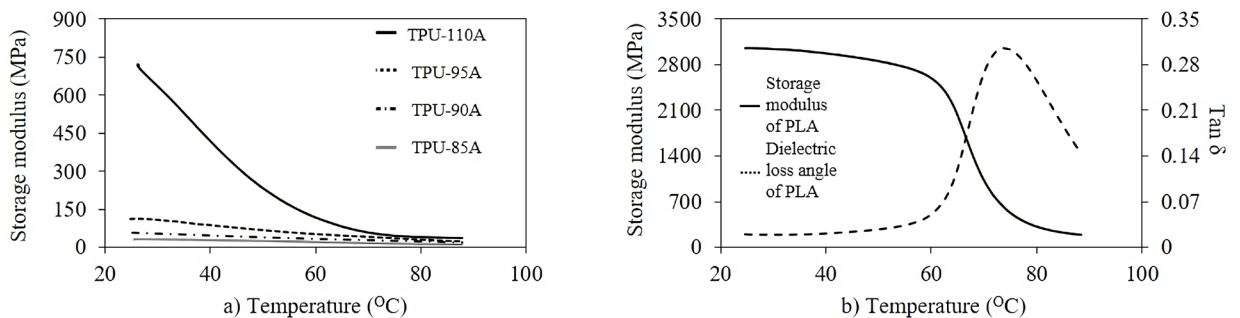


Fig. 5. DMA test results, a) storage modulus of TPU, b) storage modulus and dissipation factor angle of PLA

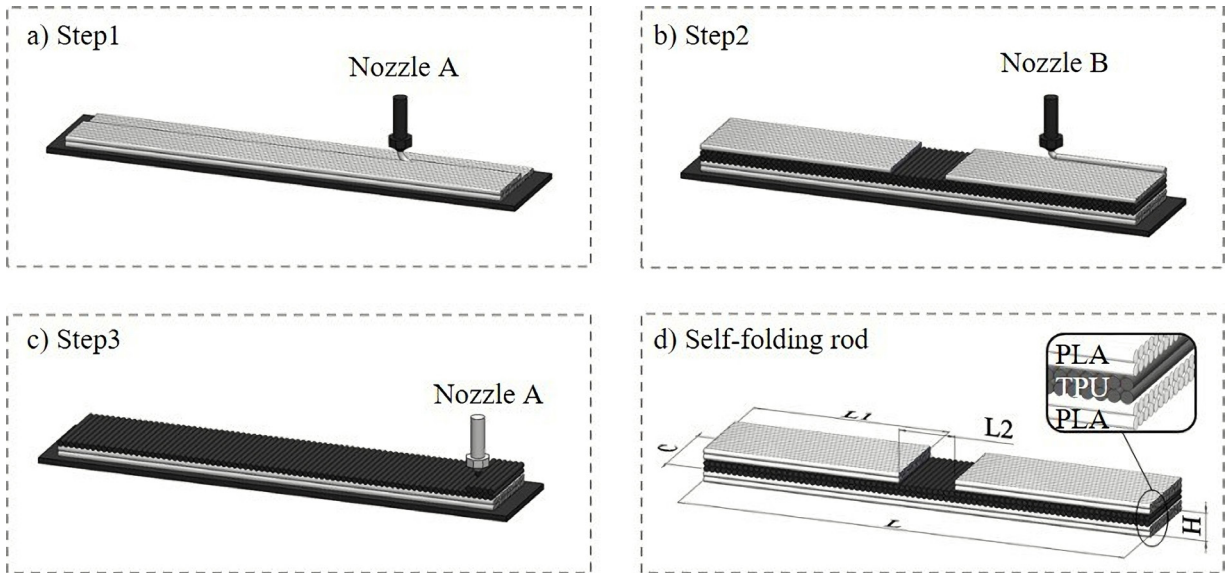


Fig. 6. Schematic of the manufacturing process of the self-folding rod; a) nozzle A print the first layer, b) nozzle B prints the second layer, c) nozzle A print the second layer, and d) self-folding rod

6). The structure consists of 6 layers, 4 of which are continuous and 2 of which are split. The separation layers are designed to control the deformed part's width and compensate for the edge bending generated by the PLA layer.

First, we explain the principle of the morphing produced by the self-folding rod. Heating and squeezing the PLA filament during the printing process cause the polymer chains to stretch and align in the direction of that path and subsequently generate stress. They are stored in the printed material due to the constraining effect of the printing platform or previous layer. They are fixed layer by layer as the printing process cools. When the PLA layers are removed from the printer and reheated above its glass transition temperature T_g , the PLA layer shortens along the printing direction and expands slightly along the other two directions. Thus, the PLA drives the structure to produce morphing.

Second, we explain how the structural design can program the self-folding rod to produce bending. PLA layers with unidirectional filling patterns exhibit anisotropic deformation behaviour, resulting in more significant anisotropic behaviours than PLA layers with multidirectional filling patterns [17] and [18]. For this reason, all PLA layers in this work are always printed in the same orientation. However, only single-layer PLA structures are used, which can produce unpredictable flexural-torsional deformations. The DMA test finds that the glass transition temperature

of TPU is generally lower than room temperature. The TPU elastic modulus is relatively stable over the T_h temperature range from room temperature to PLA, and it is assumed that it cannot contract; it can only bend and slightly elongate. Using these properties, PLA and TPU are combined in layers to form a combination structure. TPU converts the unpredictable flex-torsion of PLA into bending. Although the TPU plays a restricted role in the structure, its filling patterns also affect the morphing. The experimental results reveal that when the filling patterns of the TPU layers are perpendicular to the PLA layers, and there is no separation layer, the structure exhibited the best bending (see Fig. 7).

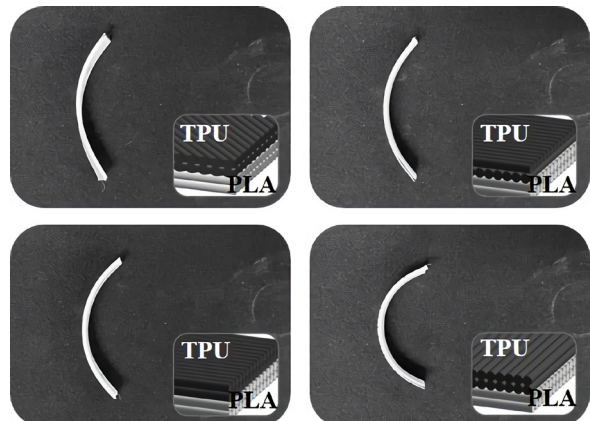


Fig. 7. Experiments on the influence of different filling patterns of TPU layer on bending deformation

3.3 Morphing Influence based on Manufacturing Parameters

After the self-folding rod bends by structural design to meet the required folding angle β and driving of the self-folding structure as much as possible, this section discusses the morphing influence of the self-folding rod under different manufacturing parameters. The previous discussion shows that releasing stored prestress in the PLA layer and the TPU layer's restriction controls the self-folding rod's bending. Therefore, if the morphing influence of the self-folding rod is obtained, it is necessary to research the effect of the restricted capability of the TPU or the prestress storage capability of the PLA on the change of the folding angle β .

First, the restricted capability of the TPU is discussed. Four self-folding rods are printed and experimented with using four TPU materials. Hot water is chosen as the activation medium for the experiments to ensure a uniform, accurate and fast heat application on the samples [21]. The glass transition temperature T_g of the PLA material selected from Fig. 5b, and the printing speed are 30 mm/s. The temperature setting of the water bath device (LICHEN-HH4, Shanghai, China) is kept constant. All samples are kept in water for the experiments, and heating stops when they no longer exhibit visual signs of deformation. The printing parameters, sample size, and experimental parameters are shown in Table 2.

Experiments find that TPU materials with higher storage modulus are more resistant to structural bending. Therefore, the high storage modulus of the TPU material causes a weak self-folding rod drive and a large folding angle β (see Fig. 8). According to another experimental result in the literature [19] to [20], the lower the percentage of hard polymer segments supporting TPU materials, the more difficult

it is to print them. After considering the printing quality and material properties, this work chose a single TPU-90A material to print the self-folding rod.

Table 2. Self-folding rod of sample structure size, printing, and experimental parameters

Structure size [mm]	H	C	$L2$	$L1$	L
	1.2	10	10	45	100
Printing parameters	Layer height [mm]				0.2
	Infill amount [%]				100
	Extrusion width [mm]				0.4
	Nozzle diameter [mm]				0.4
	Printing platform temperature [°C]				30
	PLA Printing temperature [°C]				235
	TPU Printing temperature [°C]				200
Experimental parameters	Activation medium				Water
	Water bath temperature [°C]				68
	Water bath time [s]				≥ 180

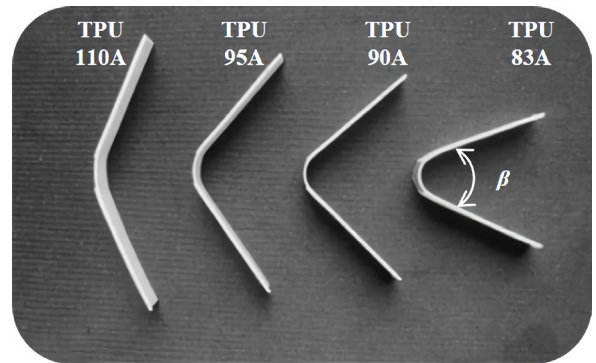


Fig. 8. Experiment on the influence of TPU layer restriction capability on the change of folding angle β

Second, the prestress storage capability of the PLA is discussed. The print speed adjustment causes different stretching of the PLA material during the extrusion process, resulting in different residual

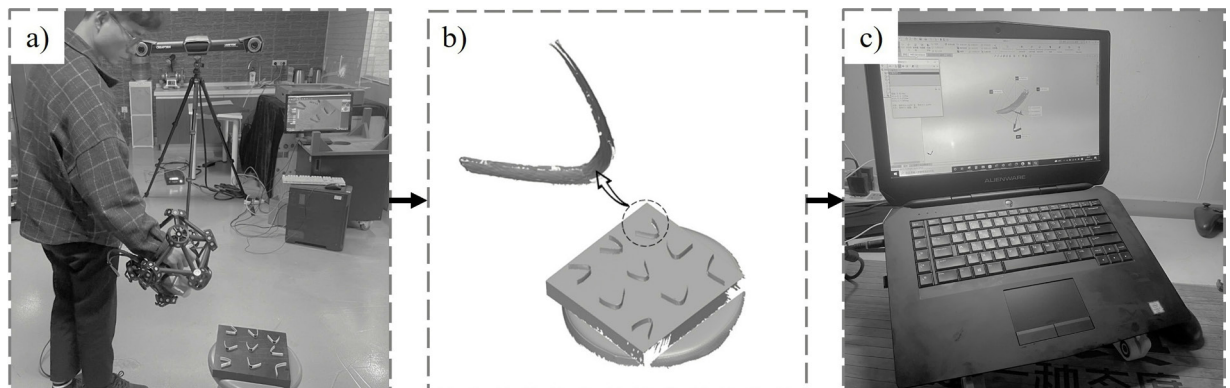


Fig. 9. 3D optical scanning processes, a) model scanning, b) model extraction, c) model measurement

stresses stored in the material. For each group of five samples, PLA layers were printed at 150 mm/s and 30 mm/s, and TPU layers at 30 mm/s. The other parameters were the same as those shown in Table 2, except for adjusting the PLA printing speed. The experimental method was the same as described before.

An optical 3D scanner (MetraSCAN 3D, Lévis, Canada) was used to measure the folding angle β after deformation for each experiment group, aiming to assess the experimental results more accurately and quantitatively. The samples are removed from the constant temperature water bath, cooled to room temperature, and placed on a scanning test bench to capture the surface shape. The collected data are combined to create a 3D model for quantitative deformation assessment (see Fig. 9).

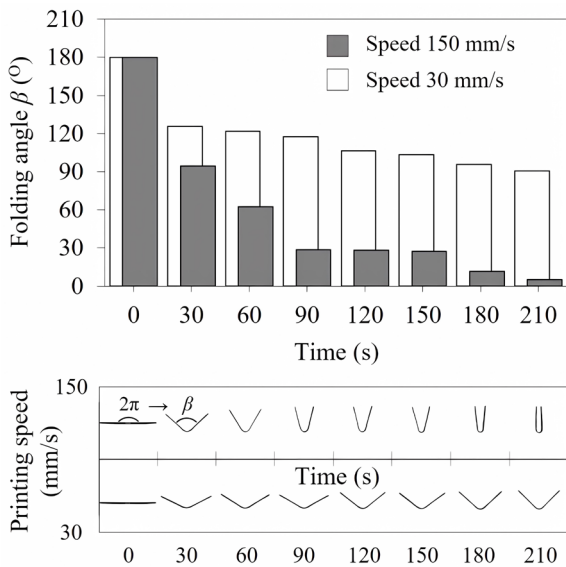


Fig. 10. Experiment on the influence of PLA layer prestress storage capability on the change of folding angle β

The average measured results of the folding angle β are shown in Fig. 10. The experimental results indicate the following:

1. Printing PLA materials at faster print speeds allow for more significant stretching polymer chain during extrusion. This approach allows the self-folding rod to maintain higher residual stresses, resulting in a broader range of folding angle variations and stronger drive capability.
2. The folding angle of the self-folding rod gradually decreases as the water bath time increases. Throughout the process, the bending is most evident in the first minute. After three minutes, the self-folding rods no longer produce significant bending, keeping their folding angle stable. Therefore, the folding capability of the self-folding rod continuously decreases with the increased water bath time.

4 MANUFACTURE AND EXPERIMENTS OF THE SELF-FOLDING COMPOSITE VARIABLE-DIAMETER WHEEL STRUCTURE

This section contains two subsections. The self-folding composite variable-diameter wheel structure with an m value of 3 is named the M3 structure. First, the M3 structure’s manufacturing is discussed, and there are simulations of the design’s viability. Second, it creates the prototype and verifies the feasibility of the M3 structural design analysis and self-adjusting wheel diameter under thermal stimulation through experiments.

4.1 Manufacture of Self-Folding Composite Variable-diameter Wheel Structure

The self-folding composite variable-diameter wheel structure is rapid-prototyped using a 3D printer. The M3 structure is constructed with 6 angulated scissor rods, 6 self-folding rods, and 2 outer hubs.

The manufacturing process needs to be described because it contains the drivable self-adjustment of the self-folding structure. The M3 structure’s folding angle β variation ranges between 180° and 120° . According to the experimental results provided in the

Table 3. Manufacturing parameters of the self-folding rods

Structure parameters	Height, H [mm]		Width, C [mm]		Separation layer width, $L1$ [mm]		Separation layer spacing distance, $L2$ [mm]		Length, L [mm]	
	1.2		10		45		10		100	
Printing parameters	Number of rod groups, m	Range of folding angle variation of 150 mm/s printing, B [°]		Range of folding angle variation for M3 structure, B [°]		PLA layer printing speed		TPU layer printing speed		Printing platform temperature, [°C]
		[180°, 5°]		[180°, 120°]		[mm/s]		[mm/s]		
	3	[180°, 5°]		[180°, 120°]		150 235		30 200		30

previous section, the self-folding rod at either of the two printing speeds can meet the design requirements of the M3 structure for the range of folding angle variations. However, in this work, a printing speed parameter of 150 mm/s is used to manufacture the self-folding rod and drive the deformation of the M3 structure to ensure that the structure obtains a significant driving force. The specific manufacturing parameters are shown in Table 3.

The angulated scissor rod and outer hub are 3D printed using a common high-temperature resistant polycarbonate material (Raise Premium, Shanghai, China). The angulated scissor rod's length B is first determined. Eq. (1) is then used to calculate the top angle α of the angulated scissor rod based on the value of m . Eq. (6) and Eq. (8) are used to calculate the radius of the theoretical unfolding and contraction of the circumcircle based on the above two parameters. Because of the thickness K limitation (see Fig. 2a), the structure does not reach the theoretical state. As a result, the radius can be increased appropriately based on the actual situation to determine the appropriate circumcircle unfolding and contraction radius. The actual circumcircle unfolding radius determines the value of R_{max} in the manufacturing of the angulated scissor rod (see Fig. 2a), and the actual circumcircle contraction radius determines the value of R_{min} in the manufacturing of the external hub. The specific manufacturing parameters of the angulated scissor rod and the outer hub in this work are shown in Table 4.

By the above manufacturing parameters, a digital M3 structure model is established, and the drivable self-adjustment of the wheel during travel is verified using Solidworks Motion. The gravitational load is 9806.65 mm/s², indicated by the green arrow. The outer hub with a rotational speed is 5 r/min, indicated by the red arrow. The ground material is chosen to be the same polycarbonate material as the outer hub, with a friction coefficient of 0.429 between each other [22]. A simplified constant force replaces the self-folding rod drive force for ease of calculation with a value of 0.75 N [23], which loads on the surface where the angulated scissor rods bond to the self-folding rods, indicated by the blue arrow. The simulation results indicate that the structure with the above designs can achieve self-folding of the wheel during travel (see Fig. 11).

4.2 Experiments of Self-Folding Composite Variable-diameter Wheel Structure

The M3 structure is manufactured according to the above parameters. The experimental verification conditions and parameter settings are consistent with previous experiments. The experimental contraction procedure is shown in Fig. 12.

Before thermal stimulation, the self-folding rod is flat, and the folding angle β reaches its maximum value. The self-folding structure unfolds in the outer hub, moving under normal wheel diameter conditions. At this moment, the circumcircle diameter of the M3

Table 4. Manufacturing parameters of the angulated scissor rods and outer hub

Structure parameters	Number of rod groups m	Top angle α [°]	Circumcircle radius				Side length B [mm]	Thickness K [mm]	Width S [mm]
			Theoretical value		Actual value				
			R_{min} [mm]	R_{max} [mm]	R_{min} [mm]	R_{max} [mm]			
	3	60	60	69.282	62	70	60	3	5

Printing parameters	Printing platform temperature [°C]	Printing speed [mm/s]	Layer height [mm]	Infill amount	Extrusion width [mm]	Printing temperature [°C]
		110	60	0.2	15%	0.4

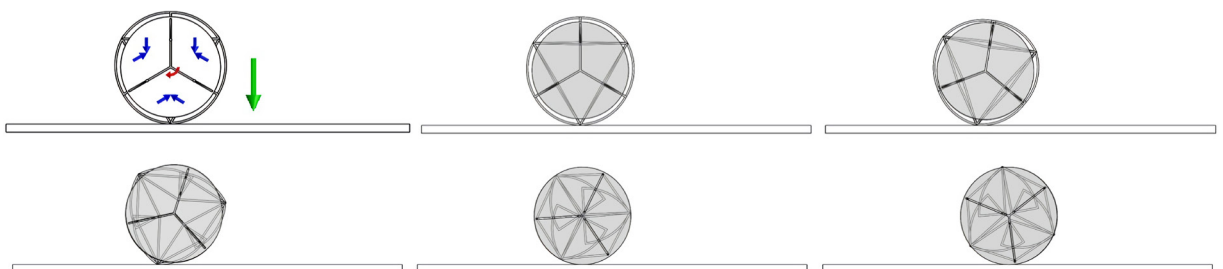


Fig. 11. The self-folding of the structure during the travelling process is obtained via simulation

structure is 140 mm (see Fig. 12a). After thermal stimulation, the self-folding rod is controllable bending, and the folding angle β reaches its minimum value. The self-folding structure moves along the outer hub track and into it.

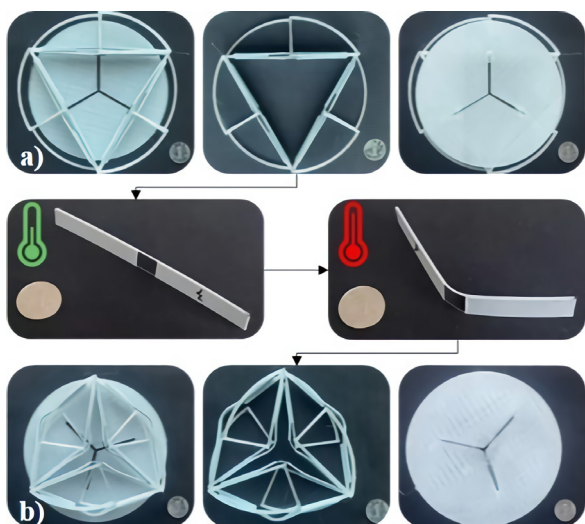


Fig. 12. Experiments of the self-folding composite variable-diameter wheel structure

The outer hub is used to achieve movement under contracting wheel diameter conditions. At this moment, the circumference diameter of the M3 structure is 124 mm (see Fig. 12b). The experimental results demonstrate that the structure can realize the self-adjusting wheel diameter under the predetermined thermal stimulation according to the set deformation control method.

5 DISCUSSION AND CONCLUSIONS

Based on 4D printing technology, we have designed a novel self-folding composite variable-diameter wheel structure. Unlike the conventional variable-diameter wheel, its novel self-folding structure combines a control system and a variable-diameter mechanical structure into one. Under predetermined thermal stimulation, the wheel diameter self-adjustment function is activated. Furthermore, we use digital prototype simulations and principle prototype experiments to validate the correctness and feasibility of the design method, theoretical analysis, and deformation control methods.

The design integrates conventional mechanical structure design, smart materials, and manufacture via 4D printing technology. A single mechanical structure design extends to a programmable morphing structure design. Compared to a conventional variable-diameter

wheel, the self-folding composite variable-diameter wheel structure designed using this new idea has less structural complexity and control difficulty.

The limitations of realistic application scenarios need to be considered. The self-folding rod within the prototype needs to be redesigned to enable bi-directional self-folding characteristics. The driving force of the self-folding rod must be redesigned to obtain bi-directional self-adjustment of the wheel diameter. The prototype should be tested in unstructured terrain and data collected on speed, time, and centrifugal force to determine parameters such as driving speed.

6 ACKNOWLEDGEMENTS

This work is funded by the National Natural Science Foundation of China (Grant No. 52175019), Beijing Natural Science Foundations (Grant No.3212009 and No.L222038), and Beijing Municipal Key Laboratory of Space-ground Interconnection and Convergence of China.

7 REFERENCES

- [1] Fu, H.X., Li, X.M., Wang, X., Ku, L.Y., Xiao, Z. (2022). Thermal mechanical coupling analysis of a flexible spoke non-pneumatic tire. *Strojniški vestnik - Journal of Mechanical Engineering*, vol. 68, no. 3, p. 143-154, DOI:10.5545/sv-me.2021.7401.
- [2] Duan, X., Huang, Q., Li, K. (2015). Design and motion characteristics analysis of small wheel-track-leg composite robot. *Journal of Mechanical Engineering*, vol. 41, no. 8, p. 108-114, DOI:10.3321/j.issn:0577-6686.2005.08.018.
- [3] Li, Y., Ge, S., Zhu, Hua., Liu, J. (2010). Mechanism and overrunning capability of four-tracked dual-swing arm robot. *Robotics*, vol. 32, no. 2, p. 157-165, DOI:10.1007/s11771-013-1460-8.
- [4] Jia, Y., Sun, Z., Zheng Y., Li, H., Tao, Z., Zhang, T., Tian, He. (2020). Overview on development of planetary rover technology. *Journal of Deep Space Exploration*, vol. 7, no. 5, p. 419-427, DOI:10.15982/j.issn.2096-9287.2020.20200031. (in Chinese)
- [5] Lee, D.Y., Kim, S.R., Kim, J.S. (2017). Origami wheel transformer: a variable-diameter wheel drive robot using an origami structure. *Soft Robotics*, vol. 4, no. 2, p. 163-180, DOI:10.1089/soro.2016.0038.
- [6] Wang, W., Zhang, Z.B., Gao, B.W. (2020). Control of tracking of two-wheeled differential spherical mobile robot. *Journal of Measurement Science and Instrumentation*, vol. 11, no. 3, p. 276-283, DOI:10.2991/jmal.2014.1.1.3.
- [7] Ma, N., Li, D.Y., He, W., Deng, Y., Li, J., Gao, Y., Bao, H., Zhang, H., Xu, X., Liu, Y., Wu, Z., Chen, L. (2021). Future vehicles: interactive wheeled robots. *Science China Information Sciences*, vol. 64, art. ID 156101, DOI:10.1007/s11432-020-3171-4.

- [8] Zhang, Z.Z., Lv, J.G., Song, B., Guo, S.Y., Gao, F. (2014). Analysis and prospect of non-pneumatic tire technology. *Tire Industry*, vol. 34, no. 9, p. 523-527.
- [9] Lee, D.Y., Kim, J.K., Sohn, C.Y., Heo, J.M., Cho, K.J. (2021). High-load capacity origami transformable wheel. *Science Robotics*, vol. 6, no. 53, art. ID abe0201, DOI:10.1126/scirobotics.abe0201.
- [10] Zhao, Y.Q., Huang, C., Jiang, C. (2013). Modeling and pass ability study of a new mechanical elastic wheel. *China Mechanical Engineering*, vol. 24, no. 6, p. 724-729.
- [11] Wang, W., Zhao, Y.G., Jiang, C., Wu, J. (2013). Analysis of mechanical transfer characteristics of a new mechanical elastic wheel. *Journal of Jiangsu University (Natural Science Edition)*, vol. 34, no. 3, p. 261-266, DOI:10.3969/j.issn.1671-7775.2013.03.003.
- [12] Zang, L.G., Zhao, Y.G., Li, B., Wang, J., Du, X.B. (2014). Analysis of mechanical elastic wheels to improve tire wear resistance and grip. *Journal of Agricultural Engineering*, vol. 30, no. 12, p. 256-263, DOI:10.3969/j.issn.1002-6819.2014.12.007.
- [13] Park, H.S., Sitti, M. (2009). Compliant footpad design analysis for a bio-inspired quadruped amphibious robot. *2009 IEEE-RSJ International Conference on Intelligent Robots and Systems*, p. 645-651, DOI:10.1109/IROS.2009.5354680.
- [14] Xie, X.L., Gao, F., Huang, C., Zeng, W. (2017). Design and development of a new transformable wheel used in amphibious all-terrain vehicles (A-ATV). *Journal of Terramechanics*, vol. 69, p. 45-61, DOI:10.1016/j.jterra.2016.11.001.
- [15] Yin, X.Y., Wang, C.W., XIE, G.M. (2012). A salamander-like amphibious robot system and control design. *2012 IEEE International Conference on Mechatronics and Automation*, p. 956-961, DOI:10.1109/ICMA.2012.6283272.
- [16] Liu, T., Yu, C.H. (1996). Identification and classification of multi-degree-of-freedom and multi-loop mechanisms. *Journal of Mechanical Design*, vol. 117, no. 1, p. 104-111, DOI:10.1115/1.2826092.
- [17] van Manen, T., Janbaz, S., Zadpoor, A.A. (2017). Programming 2D/3D shape-shifting with hobbyist 3D printers. *Materials Horizons*, vol. 6, no. 4, p. 1064-1069, DOI:10.1039/c7mh00269f.
- [18] Kačergis, L., Mitkus, R., Sinapius, M. (2019). Influence of fused deposition modeling process parameters on the transformation of 4D printed morphing structures. *Smart Materials and Structures*, vol. 28, art. ID 105042, DOI:1088/1361-665X/ab3d18.
- [19] Qi, H.J., Boyce, M.C. (2005). Stress-strain behavior of thermoplastic polyurethanes. *Mechanics of Materials*, vol. 37, no. 8, p. 817-839, DOI:10.1016/j.mechmat.2004.08.001.
- [20] Kim, K., Park, J., Suh, J.H., Kim, M., Jeong, Y., Park, I. (2017). 3D printing of multiaxial force sensors using carbon nanotube (CNT)/thermoplastic polyurethane (TPU) filaments. *Sensors and Actuators A: Physical*, vol. 263, p. 493-500, DOI:10.1016/j.sna.2017.07.020.
- [21] Hu, G., Damanpack, A.R., Bodaghi, M., Liao, W.H. (2017). Increasing dimension of structures by 4D printing shape memory polymers via fused deposition modeling. *Smart Materials and Structures*, vol. 26, art. ID 125023, DOI:10.1088/1361-665X/aa95ec.
- [22] Rubin, A., Gauthier, C., Schirrer, R. (2012). The friction coefficient on polycarbonate as a function of the contact pressure and nanoscale roughness. *Polymer Physics*, vol. 50, no. 8, p. 580-588, DOI:10.1002/polb.23046.
- [23] Yang, L. (2021). *Shape Memory Behaviors of 4D Printed Angle-Ply Laminated and Rectangular Braided Preforms and Their Composites*. Donghua University, Shanghai.